JPEDAV (2006) 27:572-581
DOI: 10.1361/154770306X153585
1547-7037/$19.00 ©ASM International

An Examination of a Multicomponent Diffusion Couple

Mysore A. Dayananda

(Submitted March 27, 2006; in revised form July 6, 2006)

New expressions relating the interdiffusion flux of a component to its own concentration gradient in a multicomponent diffusion couple have been derived and applied to a diffusion couple investigated in the Cu-Ni-Zn system. From these relations, effective interdiffusion coefficients were determined at selected sections in the diffusion zone directly from the locations of the sections relative to the Matano plane. The Cu-Ni-Zn couple was analyzed for interdiffusion fluxes and interdiffusion coefficients with the aid of "*Multi*DiFlux" program developed for the analysis of interdiffusion in multicomponent systems. The couple was examined for zero-flux plane development, interdiffusion against activity gradients, and diffusion path representation. Diffusion path slopes at selected sections in the diffusion zone were related to the interdiffusion coefficients; slopes at path ends were determined from eigenvectors evaluated from limiting ratios of interdiffusion fluxes. Expressions for internal consistency among the concentration profiles or flux profiles of the individual components were also developed in terms of the terminal alloy compositions and applied to the Cu-Ni-Zn couple in the diffusion zone.

Keywords diffusion paths, internal consistency and constraints, multicomponent diffusion

1. Introduction

Concentration profiles developed in multicomponent diffusion couples during isothermal annealing are normally analyzed for interdiffusion fluxes and interdiffusion coefficients. New analytical methods[1] have been put forward for such analysis from individual solid-solid diffusion couples, and a free and user-friendly computer software, called *Multi*DiFlux, has been developed[2] to carry out such calculations from experimental concentration profiles of couples. The *Multi*DiFlux program converts experimental concentration profiles of all components to corresponding profiles of interdiffusion fluxes and evaluates various moments of interdiffusion fluxes by appropriate integrations. From such moments calculated over selected ranges of concentrations within the diffusion zone, $(n - 1)$ independent equations are set up for each component for the determination of $(n - 1)^2$ interdiffusion coefficients valid for each selected composition range. The use of the *Multi*DiFlux program has been illustrated and discussed[3-5] with application to ternary diffusion couples in the Cu-Ni-Zn system.

This article was presented at the Multicomponent-Multiphase Diffusion Symposium in Honor of Mysore A. Dayananda, which was held during TMS 2006, 135th Annual Meeting and Exhibition, March 12-16, 2006, in San Antonio, TX. The symposium was organized by Yongho Sohn of University of Central Florida, Carelyn E. Campbell of National Institute of Standards and Technology, Richard D. Sisson, Jr., of Worcester Polytechnic Institute, and John E. Morral of Ohio State University.

Mysore A. Dayananda, School of Materials Engineering, Purdue University, West Lafayette, IN 47907. Contact e-mail: dayanand@ecn.purdue.edu.

The main purpose of this paper is to develop relations between interdiffusion fluxes and concentration gradients and explore internal constraints on concentration profiles and interdiffusion fluxes of the various components, as dictated by the terminal alloy compositions for a ternary solid-solid diffusion couple. These constraints help check the internal consistency between the concentration profiles of the various components and provide insight on the development of the diffusion path. In addition, new expressions are presented for the slope of the diffusion path at selected sections in the diffusion zone in terms of the ternary interdiffusion coefficients evaluated by the *Multi*DiFlux program. Also, the slopes at the end regions of the diffusion path are also estimated from the eigenvectors determined from the ternary interdiffusion coefficients. The various relations developed in this paper are examined with the aid of experimental concentration profiles and interdiffusion fluxes of a Cu-Ni-Zn experimental diffusion couple. The couple is also examined for the development of zero-flux planes,[6,7] crossover compositions, and internal consistency[7] and constraints among concentration profiles, interdiffusion fluxes, and the terminal alloy compositions.

2. Interdiffusion Fluxes

2.1 Determination of Interdiffusion Fluxes

For a solid-solid diffusion couple with negligible variation in the molar volume in the diffusion zone, the interdiffusion flux $\tilde{J}_i(x)$ of a component i at a section x can be determined directly from the concentration profile of the component from the relation:[6,7]

$$\tilde{J}_i(x) = \frac{1}{2t}\int_{C_i^- \text{ or } C_i^+}^{C_i(x)} (x - x_o)\, dC_i \quad (i = 1, 2, \ldots, n) \qquad \text{(Eq 1)}$$

where x_o corresponds to the location of the Matano plane and C_i^- and C_i^+ are the compositions of the terminal alloys used in the assembly of the diffusion couple. For solid-solid

couples, concentrations are functions of the Boltzmann parameter λ defined by:

$$\lambda = (x - x_o)/\sqrt{t} \quad \text{(Eq 2)}$$

and Eq 1 can be written as:

$$\tilde{J}_i\sqrt{t} = \frac{1}{2}\int_{C_i^- \text{ or } C_i^+}^{C_i(\lambda)} \lambda \, dC_i \quad (i = 1, 2, \ldots, n) \quad \text{(Eq 3)}$$

Thus, $(\tilde{J}_i\sqrt{t})$ is a function of λ and has a unique value at a given concentration level C_i within the diffusion zone. On expressing the integral on the right-hand side of Eq 3 by $K_i(\lambda)$, Eq 3 becomes:[8]

$$\tilde{J}_i = \frac{K_i(\lambda)}{2\sqrt{t}} \quad (i = 1, 2, \ldots, n) \quad \text{(Eq 4)}$$

On integrating both sides of Eq 4 with respect to time, one gets:

$$\int_0^t \tilde{J}_i dt = K_i(\lambda) \cdot \sqrt{t} = 2t \cdot \tilde{J}_i \quad \text{(Eq 5)}$$

Equation 5 implies that the cumulative or total interdiffusion flux passing through a moving plane identified at a constant concentration level C_i over a diffusion time t is $2t$ times the instantaneous $\tilde{J}_i$ at that concentration level at time t. The variation of $\tilde{J}_i$ with respect to time t at a given concentration level C_i can be obtained by differentiating both sides of Eq 4 with respect to time t; thus:

$$\left(\frac{d\tilde{J}_i}{dt}\right)_{C_i} = -\frac{1}{2}\frac{K_i(\lambda)}{2t\sqrt{t}} = \frac{-\tilde{J}_i}{2t} \quad \text{(Eq 6)}$$

2.2 Interdiffusion Flux as a Function of x and t

$\tilde{J}_i$ can be described as a function of x and t by:

$$d\tilde{J}_i = \left(\frac{\partial\tilde{J}_i}{\partial x}\right)_t dx + \left(\frac{\partial\tilde{J}_i}{\partial t}\right)_x dt \quad \text{(Eq 7)}$$

Hence, at a concentration level C_i, the variation of $\tilde{J}_i$ with time is expressed by:

$$\left(\frac{d\tilde{J}_i}{dt}\right)_{C_i} = \left(\frac{\partial\tilde{J}_i}{\partial x}\right)_t \left(\frac{\partial x}{\partial t}\right)_{C_i} + \left(\frac{\partial\tilde{J}_i}{\partial t}\right)_x \quad \text{(Eq 8)}$$

From Eq 6 and 8, one gets:

$$\tilde{J}_i = -2t\left[\left(\frac{\partial\tilde{J}_i}{\partial x}\right)_t \left(\frac{\partial x}{\partial t}\right)_{C_i} + \left(\frac{\partial\tilde{J}_i}{\partial t}\right)_x\right] \quad \text{(Eq 9)}$$

where $(\partial x/\partial t)_{C_i}$ is the velocity of propagation $v(C_i)$ of a concentration level (C_i) within the diffusion zone. From Eq 2 at a given concentration level,

$$\left(\frac{\partial x}{\partial t}\right)_{C_i} = \frac{\lambda}{2\sqrt{t}} = \frac{x - x_o}{2t} \quad \text{(Eq 10)}$$

and Eq 9 becomes:

$$\tilde{J}_i = -\left(\frac{\partial\tilde{J}_i}{\partial x}\right)_t \cdot (x - x_o) - \left(\frac{\partial\tilde{J}_i}{\partial t}\right)_x \cdot 2t \quad \text{(Eq 11)}$$

The continuity equation is given by:

$$\left(\frac{\partial\tilde{J}_i}{\partial x}\right)_t = -\left(\frac{\partial C_i}{\partial t}\right)_x \quad (i = 1, 2, \ldots, n) \quad \text{(Eq 12)}$$

However,

$$\left(\frac{\partial C_i}{\partial t}\right)_x = -\left(\frac{\partial C_i}{\partial x}\right)_t \cdot \left(\frac{\partial x}{\partial t}\right)_{C_i} \quad \text{(Eq 13)}$$

On the basis of Eq 10 and 13, Eq 12 becomes:[6,7]

$$\left(\frac{\partial\tilde{J}_i}{\partial x}\right)_t = \frac{(x - x_o)}{2t}\left(\frac{\partial C_i}{\partial x}\right)_t \quad (i = 1, 2, \ldots, n) \quad \text{(Eq 14)}$$

Equation 14 provides a direct link between the gradient of interdiffusion flux of a component to its own concentration gradient at any section x through the velocity of propagation of the concentration level (C_i) identified at the section x at time t.

On substituting Eq 14 in Eq 11, one gets:

$$\tilde{J}_i = -\frac{(x - x_o)^2}{2t}\left(\frac{\partial C_i}{\partial x}\right)_t - \left(\frac{\partial\tilde{J}_i}{\partial t}\right)_x 2t \quad \text{(Eq 15)}$$

An expression for the second derivative of $\tilde{J}_i$ with respect to x can also be obtained by differentiating Eq 14 with respect to x; thus:

$$\left(\frac{\partial^2\tilde{J}_i}{\partial x^2}\right)_t = \frac{(x - x_o)}{2t}\left(\frac{\partial^2 C_i}{\partial x^2}\right)_t + \frac{1}{2t}\left(\frac{\partial C_i}{\partial x}\right)_t \quad \text{(Eq 16)}$$

2.3 An Expression for $(\partial\tilde{J}_i/\partial t)_x$

Multiplying both sides of Eq 4 by $(x - x_o)$, one gets:

$$[\tilde{J}_i \cdot (x - x_o)] = \frac{\lambda}{2}K_i(\lambda) \quad \text{(Eq 17)}$$

Hence, the product $[\tilde{J}_i \cdot (x - x_o)]$ is a function of λ or the composition expressed by C_i. On differentiating both sides of Eq 17 with respect to λ and using Eq 4, one gets:

$$\left(\frac{d[\tilde{J}_i \cdot (x - x_o)]}{d\lambda}\right) = \tilde{J}_i\sqrt{t} + \lambda\left(\frac{d(\tilde{J}_i\sqrt{t})}{d\lambda}\right) \quad \text{(Eq 18)}$$

Since $\tilde{J}_i\sqrt{t}$ is a function of λ, Eq 14 can be expressed by:

$$\left(\frac{d(\tilde{J}_i\sqrt{t})}{d\lambda}\right) = \frac{\lambda}{2}\left(\frac{dC_i}{d\lambda}\right) \quad \text{(Eq 19)}$$

Therefore, substitution of Eq 19 in Eq 18 yields:

$$\tilde{J}_i\sqrt{t} = -\frac{\lambda^2}{2}\left(\frac{dC_i}{d\lambda}\right) + \left(\frac{d[\tilde{J}_i \cdot (x - x_o)]}{d\lambda}\right) \quad \text{(Eq 20)}$$

or equivalently:

$$\tilde{J}_i = -\frac{(x - x_o)^2}{2t}\left(\frac{\partial C_i}{\partial x}\right)_t + \left(\frac{\partial[\tilde{J}_i \cdot (x - x_o)]}{\partial x}\right)_t$$
$$(i = 1, 2, \ldots, n) \quad \text{(Eq 21)}$$

Equation 21 provides an expression for the interdiffusion flux of a component in terms of its own concentration gradient and the gradient of the function $[\tilde{J}_i \cdot (x - x_o)]$. A comparison of Eq 15 with Eq 21 yields:

$$\left(\frac{\partial \tilde{J}_i}{\partial t}\right)_x = -\frac{1}{2t}\left(\frac{\partial[\tilde{J}_i \cdot (x - x_o)]}{\partial x}\right)_t \quad \text{(Eq 22)}$$

For a solid-solid diffusion couple, plots of $[\tilde{J}_i \cdot (x - x_o)]$ versus x can be generated for each component. Such plots will invariably show locations or sections where $[\tilde{J}_i \cdot (x - x_o)]$ is a maximum or a minimum for each component on the right-hand side as well as the left-hand side of the Matano plane, as will be illustrated with an experimental ternary diffusion couple. At such sections designated by x_{ir} and x_{il}, Eq 21 becomes:

$$\tilde{J}_i = -\left[\frac{(x - x_o)^2}{2t}\left(\frac{\partial C_i}{\partial x}\right)_t\right]_{x_{ir} \text{ or } x_{il}} \quad (i = 1, 2, \ldots, n) \quad \text{(Eq 23)}$$

Equation 23 may be looked upon as a derived statement of Fick's law, where the interdiffusion flux of the component i is proportional to its own concentration gradient at the specific sections, where $(\partial[\tilde{J}_i \cdot (x - x_o)]/\partial x)_t$ goes to zero. An effective interdiffusion coefficient for component i can also be calculated directly from $(x - x_o)^2/2t$ at each of those sections.

2.4 Variation of Interdiffusion Fluxes with Concentrations

Equation 14 or equivalently Eq 19 provides an important constraint on the variation of $\tilde{J}_i$ with C_i for each component i. Dividing both sides of Eq 14 by the concentration gradient $\partial C_i/\partial x$ yields:

$$\left(\frac{\partial \tilde{J}_i}{\partial C_i}\right)_t = \frac{(x - x_o)}{2t} = \frac{\lambda}{2\sqrt{t}} \quad (i = 1, 2, \ldots, n) \quad \text{(Eq 24)}$$

Equation 24 clearly indicates that the variation of $\tilde{J}_i$ with respect to C_i at any section x is the same for all components in the diffusion zone and is identical to the velocity of propagation of the concentration level C_i. This important internal constraint governs the interdiffusion fluxes of all components and hence the development of their concentration profiles within the diffusion zone. For experimental diffusion couples in multicomponent systems, plots of $(\partial\tilde{J}_i/\partial C_i)_t$ against $(x - x_o)$ generated for each component should yield a straight line with the slope of $1/2t$. Such plots for the various components fall on the same straight line and provide a consistency check for the experimental data on concentration profiles. It is important to note that Eq 24 holds for any solid-solid or vapor-solid couple that satisfies the use of the Boltzmann parameter in the description of their concentration profiles.

3. Ternary Interdiffusion Coefficients

3.1 Eigenvalues and Eigenvectors

Based on Onsager's expression[9] for extended Fick's law, the interdiffusion flux $\tilde{J}_i$ of component i in ternary systems is given by:

$$\tilde{J}_i(x) = -\sum_{j=1}^{2} \tilde{D}_{ij}^3 \frac{\partial C_j}{\partial x} \quad (i = 1, 2) \quad \text{(Eq 25)}$$

where four ternary interdiffusion coefficients, $\tilde{D}_{11}^3$, $\tilde{D}_{12}^3$, $\tilde{D}_{21}^3$, $\tilde{D}_{22}^3$ are defined for the independent fluxes of components 1 and 2. Component 3 is chosen as the dependent concentration variable. The matrix of these coefficients identified by $\boldsymbol{D}^{(3)}$ can be diagonalized,[10,11] and the eigenvalues, d_1 and d_2, are given by:

$$d_{1,2} = \frac{1}{2}\left[\left(\tilde{D}_{11}^3 + \tilde{D}_{22}^3\right) \pm \sqrt{\tilde{D}_o}\right] \quad \text{(Eq 26)}$$

where the discriminant $\tilde{D}_o$ is:

$$\tilde{D}_o = (\tilde{D}_{11}^3 - \tilde{D}_{22}^3)^2 + 4\tilde{D}_{12}^3\tilde{D}_{21}^3 \quad \text{(Eq 27)}$$

The eigenvectors can be expressed in columnar form in a matrix given by:[12]

$$\boldsymbol{P} = \left[\begin{pmatrix} 1 \\ \beta_1 \end{pmatrix}\begin{pmatrix} \alpha_2 \\ 1 \end{pmatrix}\right]$$

where

$$\beta_1 = \frac{(d_1 - \tilde{D}_{11}^3)}{D_{12}^3} = \frac{\tilde{D}_{21}^3}{(d_1 - \tilde{D}_{22}^3)} \quad \text{(Eq 28)}$$

and

$$\alpha_2 = \frac{(d_2 - \tilde{D}^3_{22})}{D^3_{21}} = \frac{\tilde{D}^3_{12}}{(d_2 - \tilde{D}^3_{11})} \quad \text{(Eq 29)}$$

The inverse of $\boldsymbol{P}$ is:

$$\boldsymbol{P}^{-1} = \frac{1}{(1 - \alpha_2\beta_1)} \begin{pmatrix} 1 & -\alpha_2 \\ -\beta_1 & 1 \end{pmatrix} \quad \text{(Eq 30)}$$

A diagonal matrix $\boldsymbol{\Delta}^{(3)}$ can be obtained from $\tilde{\boldsymbol{D}}^{(3)}$ through a similarity transformation[12] given by:

$$\boldsymbol{P}^{-1} \cdot \tilde{\boldsymbol{D}}^{(3)} \cdot \boldsymbol{P} = \boldsymbol{\Delta}^{(3)} \quad \text{(Eq 31)}$$

where

$$\boldsymbol{\Delta}^{(3)} = \begin{pmatrix} d_1 & 0 \\ 0 & d_2 \end{pmatrix} \quad \text{(Eq 32)}$$

On the basis of Eq 31, Eq 25 can be transformed to:

$$\tilde{J}_1 - \alpha_2\tilde{J}_2 = -d_1\left(\frac{\partial C_1}{\partial x} - \alpha_2\frac{\partial C_2}{\partial x}\right) \quad \text{(Eq 33)}$$

$$-\beta_1\tilde{J}_1 + \tilde{J}_2 = -d_2\left(-\beta_1\frac{\partial C_1}{\partial x} + \frac{\partial C_2}{\partial x}\right) \quad \text{(Eq 34)}$$

where linear combinations of fluxes are proportional to linear combinations of forces through eigenvalues.

For a ternary couple characterized by constant interdiffusion coefficients, it is known[11] that the path slope $(\partial C_2/\partial C_1)$ at the ends of the diffusion path corresponds to the direction of the major eigenvector determined by β_1; that is:

$$[\beta_1 = \partial C_2/\partial C_1]_{\text{path end}} \quad \text{(Eq 35)}$$

On the basis of Eq 35, Eq 34 yields at a path end:

$$[\tilde{J}_2/\tilde{J}_1 = \beta_1 = \partial C_2/\partial C_1]_{\text{path end}} \quad \text{(Eq 35a)}$$

and Eq 33 becomes:

$$\left[\tilde{J}_1 = -d_1\frac{\partial C_1}{\partial x}\right]_{\text{path end}} \quad \text{(Eq 36)}$$

where d_1 is an eigenvalue different from $\tilde{D}^3_{11}$.

For a couple with varying $\tilde{D}^3_{ij}$, the validity of Eq 35 may be checked, provided a set of $\tilde{D}^3_{ij}$s appropriate to an end segment or region of the diffusion path can be determined and used for the determination of the local major eigenvector. If β_1 for the major eigenvector appropriate to an end segment of the diffusion path were to be identified with the $[\partial C_2/\partial C_1]_{\text{path end}}$, then Eq 35a may be checked for its validity for a couple characterized by varying $\tilde{D}^3_{ij}$ by comparing the limiting ratios of the interdiffusion fluxes of two of the components with the path slopes at the two ends of the diffusion path.

3.2 Path Slopes in Terms of Interdiffusion Coefficients at Selected Sections

3.2.1 Path Slopes Where $(\partial[\tilde{J}_i \cdot (x - x_o)]/\partial x)_t = 0$. At the sections corresponding to the locations of the relative extrema observed in the plots of $[\tilde{J}_i \cdot (x - x_o)]$ against x, the path slopes can be estimated directly from the interdiffusion coefficients and the section location. For example, at the extrema in the plot of $[\tilde{J}_1 \cdot (x - x_o)]$ against x for component 1, Eq 23 and 25 can be combined to yield:

$$\frac{\partial C_2}{\partial C_1} = \frac{(x - x_o)^2 - 2t\,\tilde{D}^3_{11}}{2t\,\tilde{D}^3_{12}} \quad \text{(Eq 37)}$$

Similarly, at the sections for the extrema of the plot of $[\tilde{J}_2 \cdot (x - x_o)]$ against x,

$$\frac{\partial C_2}{\partial C_1} = \frac{2t\,\tilde{D}^3_{21}}{[(x - x_o)^2 - 2t\,\tilde{D}^3_{22}]} \quad \text{(Eq 38)}$$

Also, at the extrema of the plot of $[\tilde{J}_3 \cdot (x - x_o)]$ against x,

$$\frac{\partial C_3}{\partial C_1} = \frac{2t\,\tilde{D}^2_{31}}{[(x - x_o)^2 - 2t\,\tilde{D}^2_{33}]} \quad \text{(Eq 39)}$$

In Eq 39 the interdiffusion coefficients are based on component 2 as the dependent variable.

3.2.2 Path Slopes at Zero-Flux Planes. At the zero-flux plane (ZFP) for a component i, $\tilde{J}_i = 0$. Therefore, Eq 25 yields:[6,7]

$$\left[\tilde{D}^3_{i1}\frac{\partial C_1}{\partial x} + \tilde{D}^3_{i2}\frac{\partial C_2}{\partial x}\right]_{\text{ZFP}} = 0 \quad \text{(Eq 40)}$$

or alternatively:

$$\left[\frac{\partial C_1}{\partial C_2}\right]_{\text{ZFP for } i} = -\frac{\tilde{D}^3_{i2}}{\tilde{D}^3_{i1}} \quad \text{(Eq 41)}$$

Thus, on the basis of Eq 41, the path slope at the ZFP is identical to the ratio of the cross to the main interdiffusion coefficients for the component exhibiting the ZFP.

4. An Examination of a Ternary Cu-Ni-Zn Diffusion Couple

4.1 The Diffusion Path, Concentration Profiles, and Flux Profiles

The diffusion path for a Cu-Ni-Zn couple[6,7] assembled with two alloys, α_5 (30.1Cu-44.7Ni-25.2Zn at.%) and α_{12} (80.6Cu-19.4Ni), with similar Ni thermodynamic activities

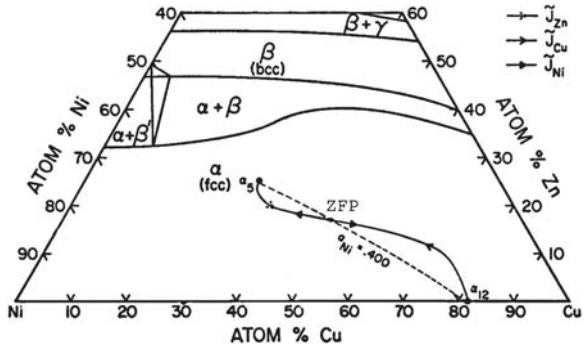

Fig. 1 Diffusion path for the Ni isoactivity couple α_5 versus α_{12} annealed at 775 °C for 2 days[6,7]

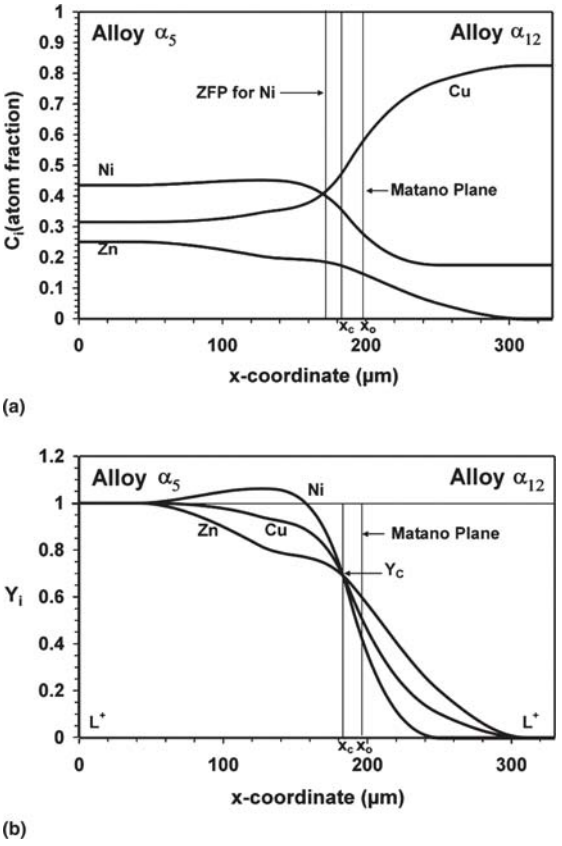

Fig. 2 Concentration profiles for the α_5 versus α_{12} Cu-Ni-Zn diffusion couple[6,7] annealed at 775 °C for 2 days. Concentrations are expressed in (a) atom fraction and (b) relative concentration variable Y_i. Y_c corresponds to the common composition at the crossover section x_c of the profiles.

and annealed at 775 °C for two days are presented in Fig. 1. The concentration profiles of the couple are presented in Fig. 2. The concentrations are expressed in atom fraction in Fig. 2(a), while in Fig. 2(b) they are expressed in terms of relative concentration variables, Y_i, defined by:

$$Y_i = \frac{C_i - C_i^+}{C_i^- - C_i^+} \quad (i = 1, 2, \ldots, n) \qquad \text{(Eq 42)}$$

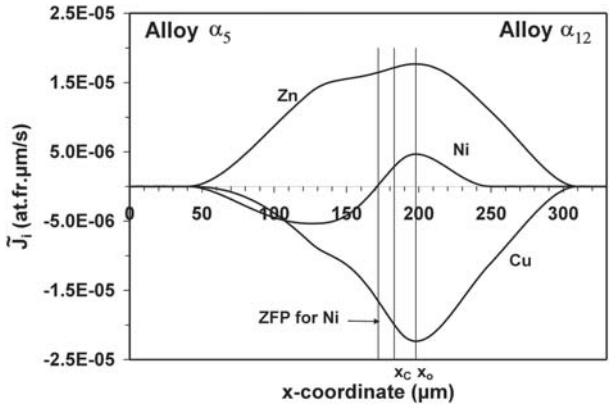

Fig. 3 Calculated profiles of interdiffusion fluxes for the α_5 versus α_{12} Cu-Ni-Zn diffusion couple annealed at 775 °C for two days

where C_i^- and C_i^+ represent the concentrations of the component i in the terminal alloys of the couple. The individual profiles clearly intersect one another at a common composition identified as Y_c at a section denoted by x_c. Also marked on the profiles is the location of the Matano plane x_o. The Ni concentration profile develops a relative maximum on the alloy α_5 side of the couple.

An advantage of Y_i versus x plot lies in the fact that the concentration profiles of all components are displayed over the diffusion zone L^- to L^+ such that Y_i is 1 at L^- and is 0 at L^+ for all components regardless of their flux directions within the diffusion zone. Also, the various profiles mutually cross one another at the common crossover composition, Y_c.[7] Equation 1 can be alternatively expressed in terms of Y_i by:[7]

$$\tilde{J}_i(x) = \frac{(C_i^- - C_i^+)}{2t}\left[Y_i \int_{-\infty}^{x} \frac{(1 - Y_i)}{V_m}\, dx + (1 - Y_i) \int_{x}^{+\infty} \frac{Y_i}{V_m}\, dx \right] \qquad \text{(Eq 43)}$$

where V_m is the molar volume. An advantage of Eq 43 is that $\tilde{J}_i$s can be determined without the need to determine the location of the Matano plane.

The concentration profiles of the couple, α_5 versus α_{12}, were analyzed by the *Multi*DiFlux program[2-5] for the determination of various quantities and parameters, including $\tilde{J}_i$s, $\tilde{D}_{ij}^3$ ($i, j = 1, 2$), eigenvalues, eigenvectors, and path slopes. Profiles of $\tilde{J}_i$s for the α_5 versus α_{12} couple were directly calculated from the concentration profiles on the basis of Eq 43 by the *Multi*Diflux program. V_m varies little in the diffusion zone and is considered constant at 7.1×10^{12} μm^3 /g · mol.[13] The interdiffusion flux profiles are presented in Fig. 3, where $\tilde{J}_i$ are in units of atom.frac.μm/s and may be converted into g · mols/μm^2/s by dividing with molar volume. The interdiffusion flux of Zn is positive (from left to right), while that of Cu is negative in the opposite direction throughout the diffusion zone. On the other hand, $\tilde{J}_{Ni}$ shows regions of both positive and negative interdiffusion fluxes going through zero at a plane identified as the zero-flux plane[6,7] for Ni. The negative $\tilde{J}_{Ni}$ indicates a region of uphill interdiffusion of Ni against its own ac-

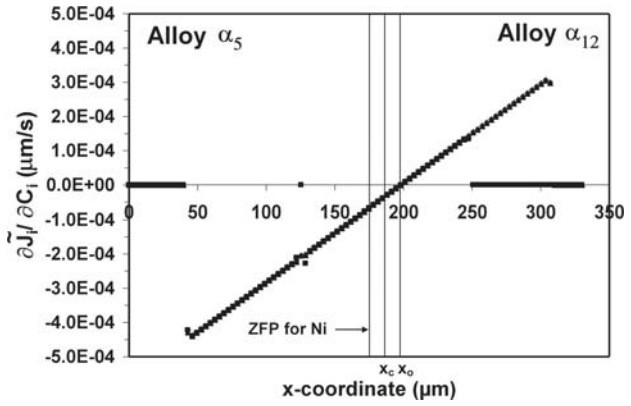

Fig. 4 Values of $(\partial[\tilde{J}_i/\partial C_i)_t$ for Zn, Ni, and Cu are plotted against x at $t = 2$ days to show that all plots fall on the same straight line with a slope of $1/2t$. ♦ = Zn; ■ = Ni; ▲ = Cu.

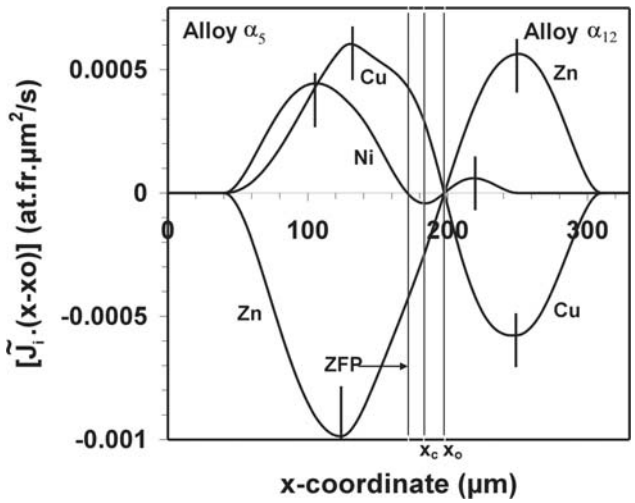

Fig. 5 Variation of $[\tilde{J}_i \cdot (x - x_o)]$ for each component i as a function of x. Each component exhibits at least one relative maximum and one relative minimum in the plots. At such sections $\tilde{J}_i$ of the component is proportional to its own concentration gradient and the effective interdiffusion coefficient is calculated directly from $(x - x_o)^2/2t$.

tivity gradient to the left of ZFP in Fig. 1. On the basis of Eq 14 $\partial \tilde{J}_i/\partial x$ for each component goes to zero at the Matano plane x_o; thus $\tilde{J}_i$ for each i exhibits a relative maximum or minimum, as can be seen from the flux profiles shown in Fig. 3.

4.2 Merging of Profiles into a Straight Line

On the basis of Eq 24, the experimental data for the profiles of the individual components can be converted into plots of $\partial \tilde{J}_i/\partial C_i$ against x. Such plots represent the variation of the velocity of propagation of the various concentration levels as a function of x at time t and yield straight lines with a slope of $1/2t$; they are shown for the couple α_5 versus α_{12} in Fig. 4. It is apparent the individual plots for Zn, Ni, and Cu fall on the same straight line over the diffusion zone, as required.

4.3 Prediction of Effective Interdiffusion Coefficients at Selected Sections

As discussed in Section 2.3, Eq 21 and 23 provide additional insights in the analysis of solid-solid diffusion couples. For the couple α_5 versus α_{12} couple, plots of $[\tilde{J}_i \cdot (x - x_o)]$ against x generated for the various components are presented in Fig. 5. For Zn and Cu this figure shows at least one section on either side of the Matano plane, where $(\partial[\tilde{J}_i \cdot (x - x_o)]/\partial x)_t$ is zero; for Ni, however, there are two such locations on the α_5 side of the couple and one section on the α_{12} side of the couple. These sections may be designated by x_{ir} and x_{il}, depending on whether they are on the right-hand side or the left-hand side of the Matano plane. At each of these sections, an effective interdiffusion coefficient for component i was calculated directly from $(x - x_o)^2/2t$ on the basis of Eq 23. These calculated values are presented in Table 1 and compared with those determined from the ratios of $[-\tilde{J}_i/(\partial C_i/\partial x)_t]$. These two sets of values show excellent agreement proving the validity of Eq 23 and consistency in the calculations. The uncertainties in the calculated interdiffusion fluxes and concentration gradients are well within 2% based on repeated calculations. Excellent reproduction of the original concentration profiles from the evaluated interdiffusion coefficients have been reported in earlier papers.[3,4]

4.4 Diffusion Path and the Crossover Composition

The diffusion path for the α5 versus α12 Cu-Ni-Zn couple is presented in terms of the relative concentrations Y_i in Fig. 6. Y_{Zn} is plotted against Y_{Cu} in Fig. 6(a), while a plot of Y_{Zn} versus Y_{Ni} is shown in Fig. 6(b). The S-shaped path crosses the straight line joining the terminal relative concentrations of 0 and 1 at the common crossover composition, Y_c. For ternary alloys characterized by negligible variation in molar volume with composition, one can write:[7]

$$Y_1 \cdot \Delta C_1 + Y_2 \cdot \Delta C_2 + Y_3 \cdot \Delta C_3 = 0 \qquad \text{(Eq 44)}$$

where ΔC_i is equal to $(C_i^- - C_i^+)$. Since

$$\sum_{i=1}^{3} \Delta C_i = 0$$

Eq 44 becomes:

$$(Y_1 - Y_3) = -\frac{\Delta C_2}{\Delta C_1}(Y_2 - Y_3) \qquad \text{(Eq 45)}$$

If $Y_1 = Y_3$ at the intersection of relative concentration profiles of two of the components, it follows from Eq 45 that $Y_2 = Y_3$. Hence, $Y_1 = Y_2 = Y_3 = Y_c$, and the relative concentration profiles of all three components intersect at a common relative concentration.

Table 1 Assessment of Eq 23 at selected sections within the diffusion zone for the α_5 versus α_{12} couple

Component	x_{min}, μm	x_{max}, μm	$\tilde{J}_i$	$(\partial C_i/\partial x)_t$	$-\tilde{J}_i/(\partial C_i/\partial x)_t$, m²/s	$(x - x_o)^2/2t$, m²/s
Zn	123		1.32E−05	−8.25E−04	1.60E−14	1.63E−14
		251	1.06E−05	−1.29E−03	8.17E−15	8.13E−15
Ni	184		3.08E−06	−5.18E−03	5.93E−16	5.67E−16
		106	−4.85E−06	1.96E−04	2.57E−14	2.45E−14
		219	2.81E−06	−2.26E−03	1.25E−15	1.28E−15
Cu	246		−1.20E−05	1.78E−03	6.73E−15	6.67E−15
		130	−8.92E−06	6.85E−04	1.30E−14	1.34E−14

4.5 Internal Consistency between Profiles

From plots of Y_i versus x for any component i, it has been shown[7] that:

$$\int_{-\infty}^{+\infty} (Y_i - Y_j)\, dx = 0 \quad (i, j = 1, 2, 3;\ i \neq j) \tag{Eq 46}$$

Equation 46 has been identified as a consistency relation[7] for the concentration profiles. Equation 46 is alternatively expressed by:

$$\int_{-\infty}^{x_c} (Y_j - Y_i)\, dx = \int_{x_c}^{+\infty} (Y_i - Y_j)\, dx \quad (i, j = 1, 2, 3;\ i \neq j) \tag{Eq 47}$$

Also, the integral $\int_x^{+\infty} (Y_i - Y_j)\, dx$ has a maximum value when $Y_i = Y_j = Y_c$ at x_c. For the α5 versus α12 couple, plots of $(Y_i - Y_j)$ versus x are presented in Fig. 7, where it can be clearly seen that for the various combinations of i and j, the hatched areas such as A and B, one on either side of x_c, correspond to the two integrals identified in Eq 47 and are equal. By expressing Eq 1 in terms of Y_i, one can derive the relation: [7]

$$\left[\frac{\tilde{J}_i}{\Delta C_i} - \frac{\tilde{J}_j}{\Delta C_j}\right]_{x_c} = \frac{1}{2t}\int_{x_c}^{+\infty} (Y_i - Y_j)\, dx \quad (i, j = 1, 2, 3;\ i \neq j) \tag{Eq 48}$$

In Fig. 7 each of the two hatched areas, equal in magnitude, is $2t$ times the weighted difference in the interdiffusion fluxes of i = Zn and j = Cu at x_c, as represented by the left-hand side of Eq 48.

4.6 Constraints on Differences of Relative Concentrations and Their Derivatives

For a solid-solid ternary diffusion couple, there exist several constraints among the relative concentration profiles of the components. Equation 45 requires that a plot of $(Y_1 - Y_3)$ versus $(Y_2 - Y_3)$ is a straight line with a unique slope of $-(\Delta C_2/\Delta C_1)$ dictated by the terminal alloy compositions. Such a plot is presented in Fig. 8 for the α5 versus α12 couple. Similarly, on differentiating Eq 45 with respect to x:

$$\frac{\partial(Y_1 - Y_3)}{\partial x} = -\frac{\Delta C_2}{\Delta C_1}\frac{\partial(Y_2 - Y_3)}{\partial x} \tag{Eq 49}$$

Similar expressions involving higher-order derivatives of $(Y_1 - Y_3)$ and $(Y_2 - Y_3)$ can also be derived from Eq 49. In Fig. 7 the plots of $(Y_i - Y_j)$ versus x show a relative minimum or a maximum at two sections, identified by x_{m1} and x_{m2}. At these sections $\partial(Y_i - Y_j)/\partial x = 0$ or:

$$\left[\frac{\partial Y_i}{\partial x} = \frac{\partial Y_j}{\partial x}\right]_{x_{m1}\text{ or }x_{m2}} \quad (i, j = 1, 2, 3;\ i \neq j) \tag{Eq 50}$$

From Eq 49 and 50 it follows that $\partial Y_1/\partial x = \partial Y_2/\partial x = \partial Y_3/\partial x$ at each of these sections, x_{m1} and x_{m2}. Equation 50 implies that at these sections the path slope $\partial C_i/\partial C_j$ is identical to $\Delta C_i/\Delta C_j$. Alternatively, the path slope $\partial Y_i/\partial Y_j$ is equal to 1 at such locations; they have been identified as points 1 and 2 on the diffusion path of the α_5 versus α_{12}, Cu-Ni-Zn diffusion couple, shown in Fig. 6.

Figure 9 presents a plot of $\partial(Y_i - Y_j)/\partial x$ with x. This plot shows the fact that the various maxima and minima in the values of $\partial(Y_i - Y_j)/\partial x$ for different combinations of i and j occur at the same section identified by x_{mm}. At this section, $\partial^2(Y_i - Y_j)/\partial x^2 = 0$ for all combinations of i and j. Also, $\partial^2 Y_i/\partial x^2$ has the same value for all components at x_{mm}, on the basis of equation similar to Eq 49 linking the second derivatives of $(Y_i - Y_j)$ with respect to x.

4.7 Constraints on Interdiffusion Fluxes

Since

$$\sum_i \tilde{J}_i = 0$$

one can write:

$$\Delta C_1 \cdot \frac{\tilde{J}_1}{\Delta C_1} + \Delta C_2 \cdot \frac{\tilde{J}_2}{\Delta C_2} + \Delta C_3 \cdot \frac{\tilde{J}_3}{\Delta C_3} = 0 \tag{Eq 51}$$

Using the relation

$$\sum_{i=1}^{3} \Delta C_i = 0$$

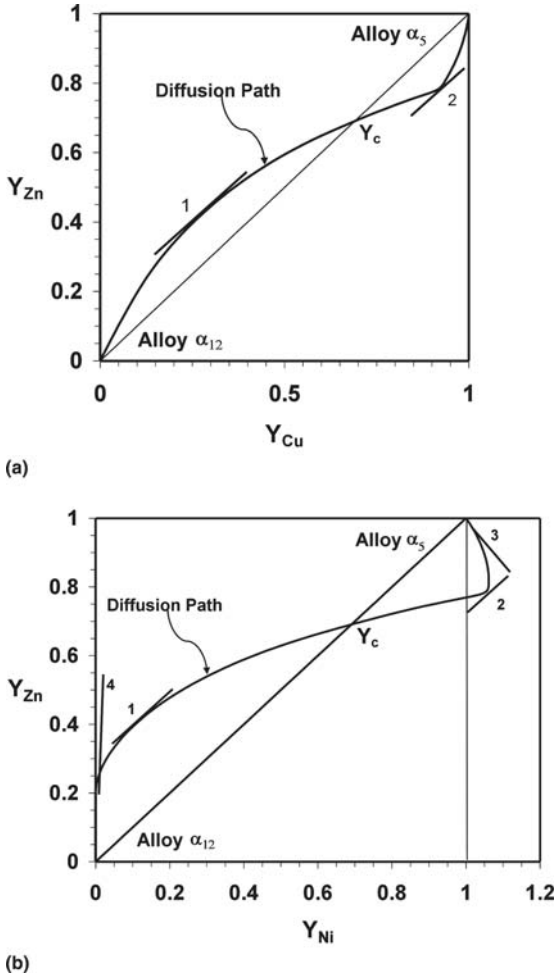

Fig. 6 Diffusion path for the α_5 versus α_{12} couple obtained by plotting (a) Y_{Zn} versus Y_{Cu} and (b) Y_{Zn} versus Y_{Ni}. The path slopes $\partial Y_i/\partial Y_j$ at points 1 and 2 are equal to 1, and slopes at points 3 and 4 are dictated by Eq 35a.

Eq 51 becomes:

$$\left[\frac{\tilde{J}_1}{\Delta C_1}-\frac{\tilde{J}_3}{\Delta C_3}\right]=-\frac{\Delta C_2}{\Delta C_1}\left[\frac{\tilde{J}_2}{\Delta C_2}-\frac{\tilde{J}_3}{\Delta C_3}\right] \quad \text{(Eq 52)}$$

A plot of $[(\tilde{J}_1/\Delta C_1) - (\tilde{J}_3/\Delta C_3)]$ versus $[(\tilde{J}_2/\Delta C_2) - (\tilde{J}_3/\Delta C_3)]$ for the $\alpha 5$ versus $\alpha 12$ couple would yield a straight line with a slope similar to the one shown in Fig. 8. Constraints similar to Eq 52 can also be derived for the derivatives of $[(\tilde{J}_i/\Delta C_i) - (\tilde{J}_j/\Delta C_j)]$ with respect to x. In addition, an integration of Eq 52 with respect to x over any selected region, x_1 to x_2 in the diffusion zone yields:

$$\int_{x_1}^{x_2}\left[\frac{\tilde{J}_1}{\Delta C_1}-\frac{\tilde{J}_3}{\Delta C_3}\right]dx=-\frac{\Delta C_2}{\Delta C_1}\int_{x_1}^{x_2}\left[\frac{\tilde{J}_2}{\Delta C_2}-\frac{\tilde{J}_3}{\Delta C_3}\right]dx \quad \text{(Eq 53)}$$

Hence, the differences in the concentrations of the components in the terminal alloys clearly relate to the differences between the interdiffusion fluxes of the individual components and their integrals.

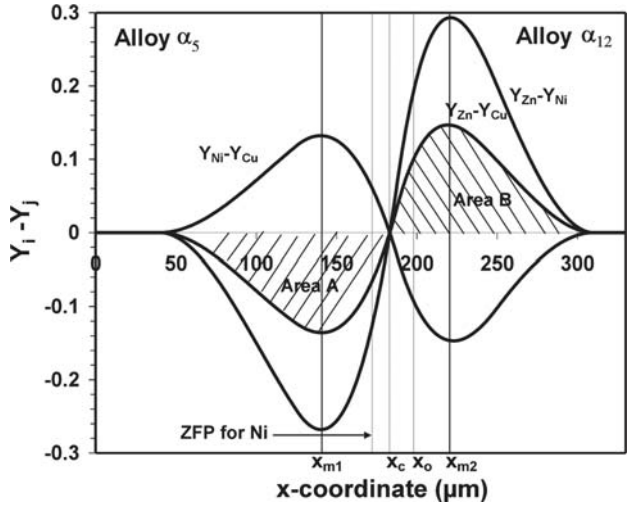

Fig. 7 Variation of $(Y_i - Y_j)$ as a function of x. (i, j = Zn, Ni, Cu, $i \neq j$). The relative maxima and minima for the various plots appear at the locations, x_{m1} and x_{m2}. Also, area A = area B, as required by Eq 47.

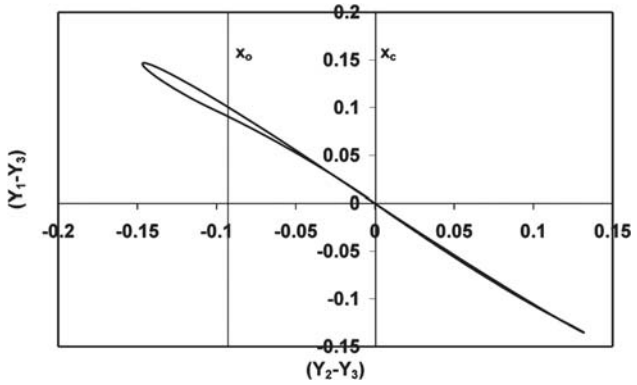

Fig. 8 Variation of $(Y_1 - Y_3)$ with $(Y_2 - Y_3)$ shows the constraint that the plot is a straight line with a slope of $-\Delta C_2/\Delta C_1$. 1 = Zn; 2 = Ni; 3 = Cu.

4.8 Interdiffusion Fluxes and the Path Slopes at the Diffusion Path Ends

Average values of ternary interdiffusion coefficients, $\tilde{D}^3_{11}$, $\tilde{D}^3_{12}$, $\tilde{D}^3_{21}$, $\tilde{D}^3_{22}$, (1 = Zn; 2 = Ni; 3 = Cu) determined for the $\alpha 5$ versus $\alpha 12$ couple with the aid of the *Multi*DiFlux program for the two regions, one on either side of the Matano plane, are reported in Table 2. The details of such calculations and their use for error function representation of the concentration profiles have been discussed in earlier papers.[3,4] Also included in Table 2 are the actual path slopes $[\partial C_1/\partial C_2]_{\text{path end}}$ determined at the end segments of the diffusion path. These slopes are found to correspond to the limiting ratios of $\tilde{J}_1/\tilde{J}_2$.

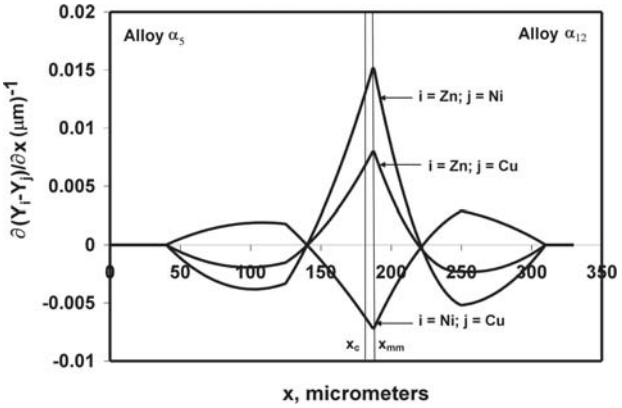

Fig. 9 Variation of $\partial(Y_i - Y_j)/\partial x$ with x for various combinations of i and j showing that the maxima and minima in the various plots appear at the same section, x_{mm}.

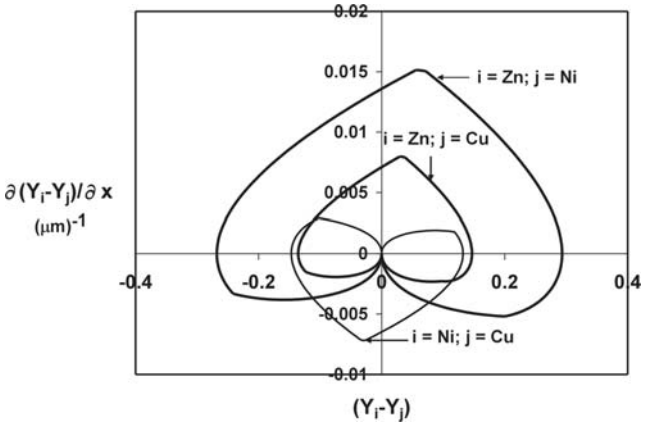

Fig. 10 Variation of $\partial(Y_i - Y_j)/\partial x$ with $(Y_i - Y_j)$ for various choices of i and j bringing out the intrinsic beauty in an artistic representation of valentine heart-shaped plots

Table 2 Calculated ternary interdiffusion coefficients for the α_5 versus α_{12} couple for two regions, one on either side of the Matano plane, and the path slopes at the ends of diffusion path

x-range, μm	Interdiffusion coefficients $\tilde{D}_{ij}^{Cu}$ (10^{-15} m^2/s)				Path end location, μm	Path slope at ends $(\partial C_{Zn}/\partial C_{Ni}) = \tilde{J}_{Zn}/\tilde{J}_{Ni}$
	$\bar{\bar{D}}_{ZnZn}^{Cu}$	$\bar{\bar{D}}_{ZnNi}^{Cu}$	$\bar{\bar{D}}_{NiZn}^{Cu}$	$\bar{\bar{D}}_{NiNi}^{Cu}$		
0-198	13.6	1.5	−5.7	1.6	$x = 0$	−1.35 on the α_5 side
198-330	5.6	2.4	0	1.1	$x = 330$	∞ on the α_{12} side

4.9 An Artistic Representation of Multicomponent Diffusion

The variables $(Y_i - Y_j)$ and $\partial(Y_i - Y_j)/\partial x$ that appear in Eq 45 and 49 can be used to generate alternative representation of interdiffusion in multicomponent systems. Such plots are presented in Fig. 10, as they bring out the inherent beauty and the internal constraints underlying the relative diffusion behavior of the various diffusing components. Figure 10 shows valentine heart-shaped plots whose sizes reflect the ratio, $\Delta C_i/\Delta C_j$, for the various combinations of i and j. The inclination of the apex of the hearts is governed by the location of the section x_{mm} in Fig. 9, where $\partial(Y_i - Y_j)/\partial x$ is an extremum for all combinations of i and j. The details of such plots will be presented in a separate paper.

5. Concluding Remarks

In this paper, new expressions have been derived for linking the interdiffusion flux of a component in a multicomponent system to its own concentration gradient without invoking Fick's law. Such relations allow the prediction of effective interdiffusion coefficients for the individual components at several selected sections within the diffusion zone directly from the locations of the sections relative to the Matano plane. These selected sections correspond to the relative extrema observed in the plots of $[\tilde{J}_i \cdot (x - x_o)]$ against x. For ternary couples the area between the profiles of relative concentrations of any two components, i and j, is identical on either side of the crossover composition. Differences in the relative concentrations or interdiffusion fluxes of any two of the components at any section can be related to similar differences for other choices of two components through concentration differences between the terminal alloys. Such relations are applicable to all sections in the diffusion zone. From a diagonalization of the matrix of ternary interdiffusion coefficients, linear combinations of interdiffusion fluxes of two of the components are found to be directly proportional to linear combinations of two of the concentration gradients through eigenvalues. Furthermore, new relations have been presented for the estimation of slopes of the ternary diffusion path at several selected sections within the diffusion zone. The limiting path slopes at the end segments are linked to the limiting ratio of the interdiffusion fluxes. Several internal constraints among the concentration profiles and interdiffusion fluxes have also been explored in terms of the terminal alloy compositions and applied to a Cu-Ni-Zn diffusion couple for internal consistency and artistic representation of multicomponent diffusion. The analysis was aided by the use of a recently developed, free computer code called *Multi*DiFlux, which can analyze the concentration profiles of multicomponent diffusion couples for interdiffusion fluxes, interdiffusion coefficients, and diffusion path representation.

Acknowledgment

This work was supported by the National Science Foundation under Grant No. DMR-0304777. Sincere thanks are expressed to Mr. Kevin Day for his help in the calculation of interdiffusion coefficients.

References

1. M.A. Dayananda and Y.H. Sohn, A New Analysis for the Determination of Ternary Interdiffusion Coefficients from a

Single Diffusion Couple, *Metall. Trans. A,* 1999, **30A,** p 535-543

2. M.A. Dayananda and L.R. Ram-Mohan, https://engineering.purdue.edu/MSE/FacStaff/Faculty/dayananda.wshtml, Purdue University, 2006
3. M.A. Dayananda, Analysis of Multicomponent Diffusion Couples for Interdiffusion Fluxes and Interdiffusion Coefficients, *J. Phase Equilib. Diffus.,* 2005, **26**(5), p 441-446
4. K.M. Day, L.R. Ram-Mohan, and M.A. Dayananda, Determination and Assessment of Ternary Interdiffusion Coefficients from Individual Diffusion Couples, *J. Phase Equilib. Diffus.,* 2005, **26,** p 579-590
5. M.A. Dayananda and K.M. Day, Analysis of Cu-Ni-Zn Ternary Diffusion Couples Using the *Multi*DiFlux Program, *TMS Lett.,* 2005, **2**(3), p 97-98
6. M.A. Dayananda and C.W. Kim, Zero-Flux Planes and Flux Reversals in Cu-Ni-Zn Diffusion Couples, *Metall. Trans. A*, 1979, **10A**(9), p 1333-1339
7. M.A. Dayananda, Analysis of Concentration Profiles for Fluxes, Diffusion Depths, and Zero-Flux Planes in Multicomponent Diffusion, *Metall. Trans. A,* 1983, **14A**(9), p 1851-1858
8. M.A. Dayananda, Average Effective Interdiffusion Coefficients and the Matano Plane Composition, *Metall. Mater. Trans. A,* 1996, **27A,** p 2504-2509
9. L. Onsager, Theories and Problems of Liquid Diffusion, *Ann. N.Y. Acad. Sci.,* 1945, **46,** p 241-265
10. H.L. Toor, Solution of the Linearized Equations of Multicomponent Mass Transfer: II. Matrix Methods, *AIChE, J.,* 1964, **10,** p 460-465
11. P.K. Gupta and A.R. Cooper Jr., The [*D*] matrix for Multicomponent Diffusion, *Phys.,* 1971, **54,** p 39-59
12. L.R. Ram-Mohan and M.A. Dayananda, A Transfer Matrix Method for the Calculation of Concentrations and Fluxes in Multicomponent Diffusion Couples, *Acta Mater.,* 2006, **54,** p 2325-2334
13. G.A. Chadwick and B.B. Argent, The Lattice Parameters of the α-Solid Solutions of the Cu-Zn-Ni and Cu-Zn-Mn, *J. Inst. Met.,* 1959-60, **88,** p 318